

RESEARCH LETTER

10.1002/2015GL066141

Key Points:

- AW circulation influenced by both local and remote wind forcing
- Remote winds force high-frequency variability in AW inflow to Arctic
- Beaufort Gyre transfers modified influence of winds to AW layer

Correspondence to:

C. Lique,
camille.lique@ifremer.fr

Citation:

Lique, C., and H. L. Johnson (2015), Is there any imprint of the wind variability on the Atlantic Water circulation within the Arctic Basin?, *Geophys. Res. Lett.*, 42, 9880–9888, doi:10.1002/2015GL066141.

Received 9 SEP 2015

Accepted 30 OCT 2015

Accepted article online 4 NOV 2015

Published online 19 NOV 2015

Is there any imprint of the wind variability on the Atlantic Water circulation within the Arctic Basin?

Camille Lique^{1,2} and Helen L. Johnson¹

¹Department of Earth Sciences, University of Oxford, Oxford, UK, ²Ifremer, Laboratoire de Physique des Océans, UMR6523, CNRS-IFREMER-IRD-UBO, Brest, France

Abstract The Atlantic Water (AW) layer in the Arctic Basin is isolated from the atmosphere by the overlying surface layer, yet observations have revealed that the velocities in this layer exhibit significant variations. Here analysis of a global ocean/sea ice model hindcast, complemented by experiments performed with an idealized process model, is used to investigate what controls the variability of AW circulation, with a focus on the role of wind forcing. The AW circulation carries the imprint of wind variations, both remotely over the Nordic and Barents Seas where they force the AW inflow variability, and locally over the Arctic Basin through the forcing of the wind-driven Beaufort Gyre, which modulates and transfers the wind variability to the AW layer. The strong interplay between the circulation within the surface and AW layers suggests that both layers must be considered to understand variability in either.

1. Introduction

The intermediate layer of the Arctic Ocean (between ~200 and 800 m) is composed of warm ($T > 0^{\circ}\text{C}$) and salty water of Atlantic origin (hereafter Atlantic Water, AW) [e.g., *Coachman and Barnes*, 1963]. This AW layer contains a large amount of heat, which, if brought to the surface, has the potential to melt all the Arctic sea ice within a few years [*Turner*, 2010]. However, the AW layer is isolated from the surface by an upper polar mixed layer [*Rudels et al.*, 1996] lying atop a strongly salinity-stratified layer (the cold halocline) [e.g., *Aagaard et al.*, 1981]. The existence of these two distinct surface and AW layers is maintained by the low level of vertical mixing [*Guthrie et al.*, 2013; *Rippeth et al.*, 2015], which permits only a small vertical heat flux from the AW layer to the surface layer throughout most of the Arctic Basin [*Lique et al.*, 2014; *Shaw and Stanton*, 2014].

Within the Arctic Basin, AW primarily circulates beneath the fresh surface layer within a cyclonic pan-Arctic current, which splits up into different branches and flows along the slope, following the different topographic features around the Eurasian and Canadian Basins [e.g., *Rudels et al.*, 1999]. Despite recent observational [*Dmitrenko et al.*, 2015; *Rudels et al.*, 2015] and modeling [*Aksenov et al.*, 2011; *Spall*, 2013; *Itkin et al.*, 2014; *Lique et al.*, 2015] efforts to improve our knowledge of the AW current, our understanding of the forcing mechanisms of both the mean and the variability of the AW current intensity remains rather crude. Previous studies have underlined the possible role of remote forcing outside of the Arctic Basin, through the input of potential vorticity [*Yang*, 2005; *Karcher et al.*, 2007] or wind forcing [*Aksenov et al.*, 2011; *Peralta-Ferriz et al.*, 2011, 2014] in the Nordic and Barents Seas. Within the Arctic Basin, the AW layer is thought to lie too deep in the water column to directly feel the influence of the wind and its variations.

In addition to the remote wind forcing, the intensity of the circulation in the AW layer is likely modulated by the strength of the surface Beaufort Gyre in the Canadian Basin. The analysis of AW circulation in several coupled ocean/sea ice models, together with isotope tracer observations, suggests that changes in the wind-driven surface layer circulation (and its associated Ekman downwelling of the isopycnals) may limit or even reverse the circulation in the AW layer on decadal and longer timescales [*Karcher et al.*, 2007, 2012]. Using an idealized process model of the Arctic to gain a better mechanistic understanding of the interplay between the intensity of the surface and intermediate layer circulations, *Lique et al.* [2015] showed that the mean strength of the AW current, while primarily set by the intensity of the AW inflow to the basin, is strongly influenced by the strength of the gyre in the surface layer, which itself depends linearly on the magnitude of the surface stress [*Davis et al.*, 2014; *Lique et al.*, 2015]. In the present study, we extend the results presented in *Lique et al.* [2015], as we investigate how variability in the wind stress over the Canadian Basin might generate variability in the AW boundary current in this region.

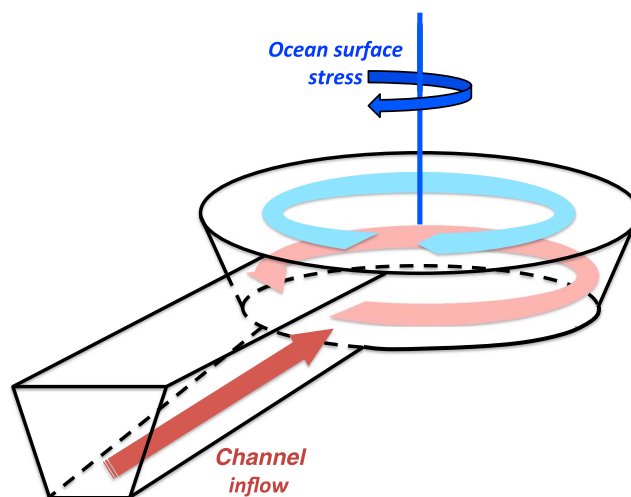


Figure 1. Schematic of the idealized process model. The circular basin is connected to a channel and has a slope all around. The surface layer is forced with an anticyclonic surface stress, resulting in a wind-driven anticyclonic gyre (similar to the Beaufort Gyre). The intermediate layer is forced with a middepth warm inflow through the channel, which results in a cyclonic boundary current flowing along the slope in the circular basin. In our sensitivity experiments, time variability is added to the surface stress, the inflow, or both.

2. Model Description

Here we use two complementary approaches using two types of numerical model. First, we analyze the output from a hindcast performed with the global ORCA025 coupled ocean/sea ice model configuration developed by the European Drakkar project [Barnier *et al.*, 2006]. The model is an implementation of the Nucleus for European Modelling of the Ocean (NEMO) [Madec, 2008] ocean/sea ice model. The configuration uses a 0.25° tripolar grid, resulting in increased resolution down to 12 km in the Arctic region and 75 uneven vertical levels. The simulation used in the present study runs from 1958 to 2010 and is initialized from rest using the Polar Science Center hydrographic temperature and salinity climatology [Steele *et al.*, 2001]. The forcing data set is the Drakkar forcing set 4 (which is an updated version of the fields described in Brodeau *et al.* [2010]). A similar setup has been successfully used in several other Arctic studies [Lique *et al.*, 2009, 2010; Popova *et al.*, 2010; Clement-Kinney *et al.*, 2014], including detailed investigations of the heat content variability within the AW layer [Lique and Steele, 2012, 2013; Dmitrenko *et al.*, 2015], and more details about the numerical design as well as extended evaluation of the ocean and sea ice model components can be found in these different papers.

We complement the analysis of the model hindcast with a set of simulations performed with an idealized process model, which only encompasses the essential physical processes and thus allows us to dismantle the dynamics at play. The model used here is identical to the one described in Lique *et al.* [2015], where details of the model setup, forcing, and results from the *Control* run (which is the same as the one used here, albeit run for 50 years instead of 10) can be found. Briefly, the Massachusetts Institute of Technology primitive equation general circulation model (MITgcm) [Marshall *et al.*, 1997] is set up in a circular semienclosed domain, connected via a channel to a sponge region which allows inflow and outflow to the basin. There is a slope all around the boundary (Figure 1). The grid has a horizontal resolution of 15 km and 30 evenly spaced vertical levels of 50 m. An anticyclonic surface stress is applied at the ocean surface representing the forcing resulting from the wind over the Arctic and the partial sea ice cover [Davis *et al.*, 2014; Lique *et al.*, 2015]. The stress field is chosen so that its curl reaches a maximum magnitude in the center of the domain and decreases to zero at the boundaries and in the outflow region. The curl field is normalized between 0 and 1 and then multiplied by a constant (which is thus the scaling factor for both ocean surface stress and the ocean surface stress curl). In the *Control* run, this constant (hereafter referred to as the maximum surface stress) is set to 0.02 N m^{-2} , resulting in a steady state anticyclonic gyre with a maximum sea surface height (SSH) of 0.6 m in the center of the basin at the end of the simulation. A cyclonic boundary current along the slope is generated in the intermediate layer by applying a strong restoring toward prescribed velocity and temperature profiles in a small part of the sponge region. This results in inflow volume and heat transports through the channel of 7 sverdrup (Sv) and 35 TW (relative to a reference temperature of 0°C), respectively, for the steady state of the

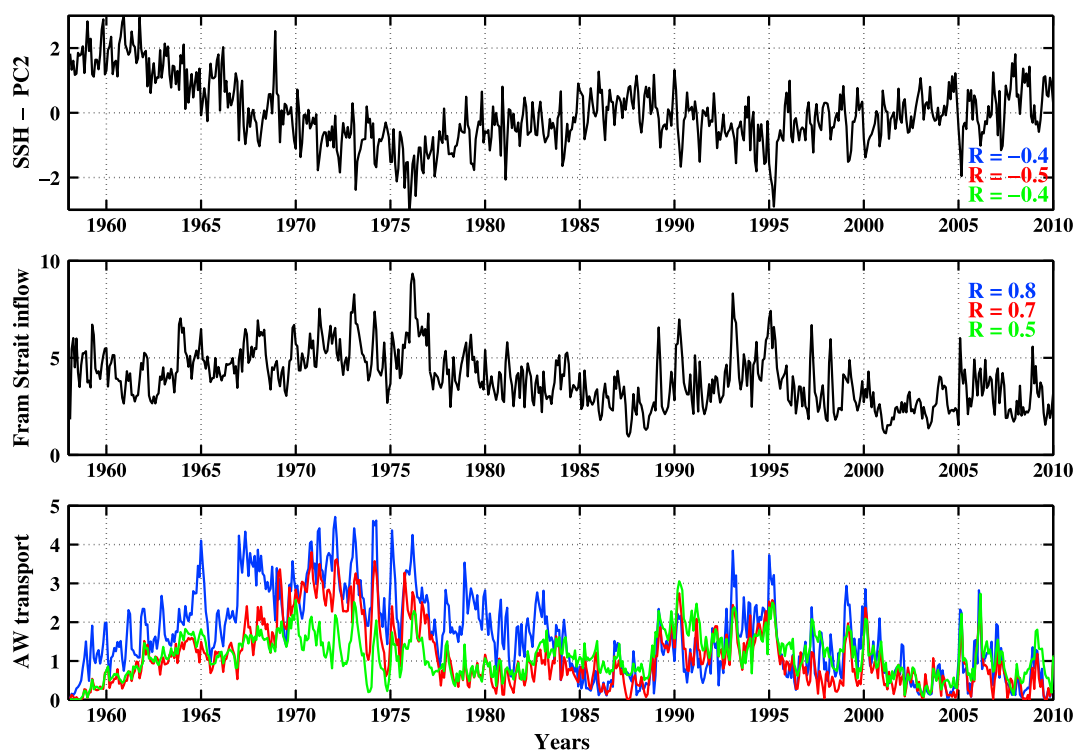


Figure 2. Time series from the Drakkar hindcast of (top) the PC of the second SSH EOF (see Figure 3a for the spatial pattern of this mode), (middle) the AW inflow through Fram Strait (in Sv), and (bottom) the transport of the AW current at three different locations around the boundary, indicated by lines of the same colors on Figure 3a. The correlations indicated in Figure 2 (top and middle) are the correlations between the time series in that panel and the three time series shown in Figure 2 (bottom).

Control experiment. These values are roughly comparable to the volume and heat transports of the AW inflow observed through Fram Strait [Schauer *et al.*, 2008; Tsubouchi *et al.*, 2012].

In addition to the *Control* experiment, we perform a series of three sensitivity experiments in which we add some time variability to either the surface stress (run labeled as *Wind*) or the inflow through the channel (run labeled as *Inflow*), or both (run labeled as *All forcing*). All simulations are run for 50 years, allowing a full dynamical adjustment in the basin. The forcing time series are constructed from a 50 year monthly time series of normally distributed random numbers. When added to the steady forcing of the *Control* run, this ensures a mean forcing identical to the *Control* run, with a standard deviation of 0.1 N m^{-2} for the surface stress (which results in a SSH standard deviation of 0.06 m, consistent with the ~ 10 cm seasonal cycle amplitude observed by satellites in the Beaufort Gyre (T. Armitage, personal communication, 2015)), and a standard deviation of 1 Sv for the inflow through the channel, consistent with the transport variations observed through Fram Strait [Schauer *et al.*, 2008; Fieg *et al.*, 2010].

3. Results From the Ocean/Sea Ice Model Hindcast

We first examine the variability of the AW boundary current in the Canadian Basin in the Drakkar hindcast. Time series of the AW current transport (defined as the transport associated with water warmer than 0°C and flowing cyclonically on the slope) are shown for three different sections around the basin in Figure 2 (the position of the three sections is shown on Figure 3a). The transport at each location exhibits a similar mean (between 1.1 and 1.6 Sv) and variability (standard deviation between 0.6 and 1 Sv), and there is some coherence in their variability (correlations between two sections range from 0.6 to 0.8 and are maximum without any lag). Despite some differences in the variability between sections (suggesting that local conditions matter), the high correlation suggests that a large fraction of the AW transport variability through the three sections around the Canadian Basin arises from a common origin.

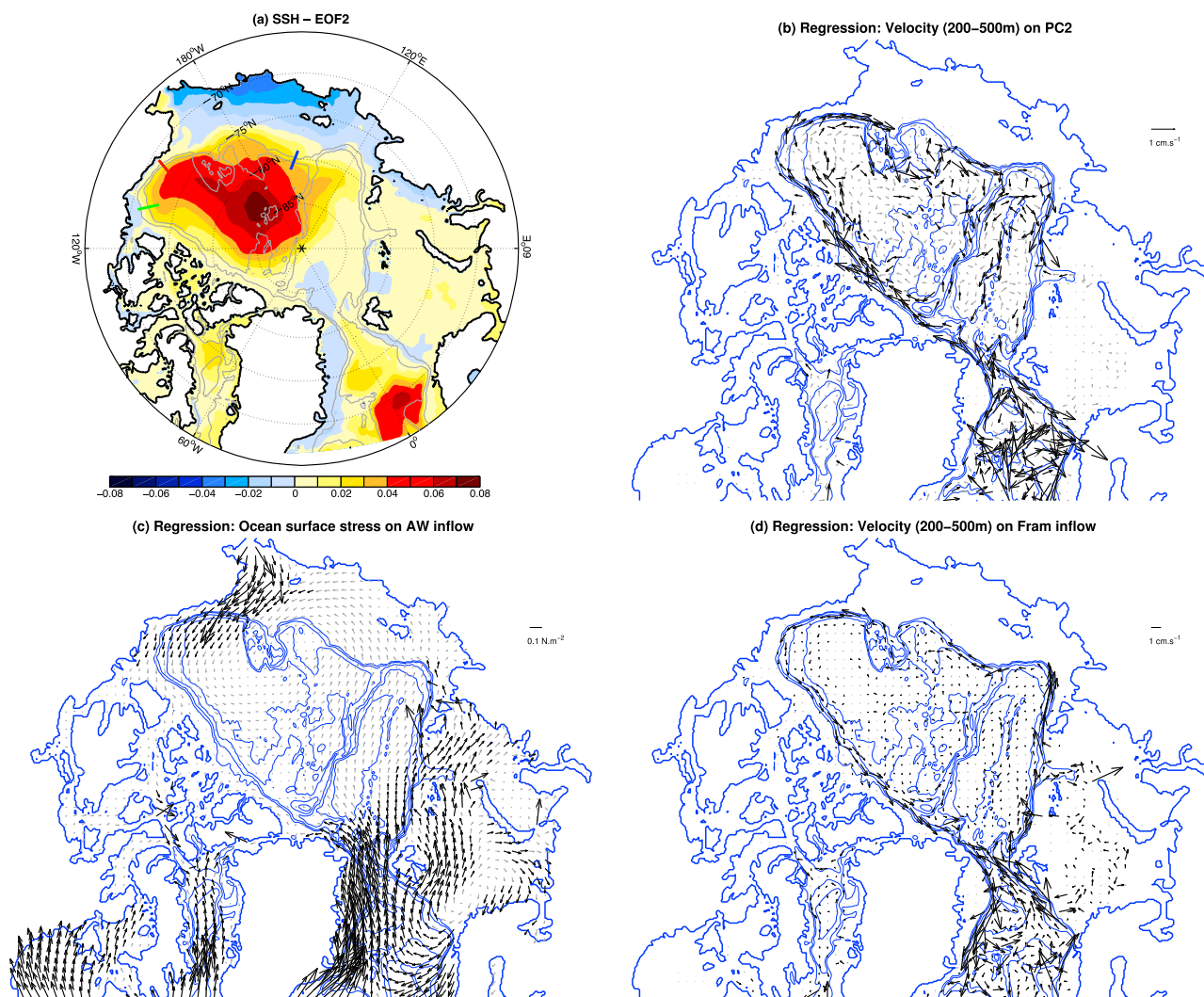


Figure 3. Results from the Drakkar hindcast. (a) Spatial pattern of the second mode of SSH variability (in m), with the sections across which AW transport is calculated indicated by short colored lines (blue, red, and green), and the 500 and 2000 m isobaths indicated in grey. (b) Regression of the velocity averaged between 200 and 500 m (i.e., in the AW layer) on PC2 of the SSH. (c) Regression of the ocean surface stress on the time series of the inflow through Fram Strait. (d) Regression of the velocity averaged between 200 and 500 m on the time series of the inflow through Fram Strait. The black arrows indicate where the regression is significant at the 95% level.

Analyzing model outputs from a roughly similar Drakkar simulation, *Lique and Steele* [2012] demonstrated coherent variations of the velocity along the slope of the Eurasian Basin at the depth of the AW core, with a strong seasonal cycle of the velocity, varying with the same phase everywhere in the basin. The high correlation between the transport of AW across different sections in the Canadian Basin, as well as the high correlation with the inflow of AW through Fram Strait (Figure 2b; the correlations between the Fram Strait inflow and the transport through the different sections range between 0.5 and 0.8, maximum without any lag), suggest that a coherent mode of variability is at play in both the Eurasian and the Canadian basins. This is further confirmed when we examine the regression of mean velocities within the AW layer (averaged between 200 and 500 m) upon the AW transport time series through Fram Strait (Figure 3d).

The regression of ocean surface stress upon the AW transport time series through Fram Strait (Figure 3c) shows a link between the anomalies of the inflow and the surface stress (which reflect anomalies of wind stress and sea ice conditions) over the Nordic and the Barents Seas. Similar patterns emerge in the regression of the ocean surface stress upon the time series of AW transport across the different sections in the Canadian Basin (not shown). The pattern found here is very similar to the regression of the winds upon the main mode of variability for the pan-Arctic ocean bottom pressure derived from the Grace satellite measurement, which is

thought to be a wintertime basin-coherent Arctic mass change driven by southerly winds through Fram Strait [Peralta-Ferriz *et al.*, 2014]. Hence, a significant part of the AW current variability in the Canadian Basin appears to be forced by remote wind variations outside of the Arctic Basin.

Can we detect any imprint of the wind time variations over the Arctic Basin itself on the AW current in the Drakkar hindcast? Using an idealized process model of the Arctic, Davis *et al.* [2014] and Lique *et al.* [2015] found that the circulation in the surface layer adjusts to a change in forcing on a ~ 15 year timescale, which arises from the balance between Ekman pumping and an eddy-induced volume flux toward the boundary of the basin. The adjustment of the AW layer to a change in wind occurs in two steps: an initial fast adjustment over a few months reflecting the propagation of boundary-trapped waves in response to a change in the inflow to the basin resulting from the wind variability outside the basin, followed by a longer adjustment which is the signature of the dynamical adjustment to wind variability over the Canadian Basin in the surface layer [Lique *et al.*, 2015]. As such, we would not expect any imprint of short-timescale variability in winds over the Canadian basin on the intermediate layer circulation and to our knowledge none has been demonstrated as yet.

We proceed by first identifying the primary modes of variability of the monthly mean SSH field in the hindcast using empirical orthogonal function (EOF) analysis. The first mode of variability (35% of the total variance) shows a pattern with positive anomalies in the interior of the basin and negative anomalies on the shelves (not shown), which is very similar to the first mode of SSH variability computed by Koldunov *et al.* [2014], and thought to be the signature of a pan-Arctic mass redistribution between the shelves and the interior, likely driven by variations in freshwater exchange with the North Atlantic. The second mode of variability (18% of the total variance) exhibits a strong loading pattern in the Canadian Basin (Figure 3a) reflecting changes in the strength of the wind-driven Beaufort Gyre, again consistent with the results of Koldunov *et al.* [2014]. Here we use the principal component (PC) time series of this second mode (Figure 2a) as a proxy for variations in the intensity of the surface layer circulation.

The time series of PC2 and the intensity of the AW current through the different sections in the Canadian Basin are anticorrelated (Figure 2, correlation coefficients between -0.4 and -0.5 depending on the section, maximum without any lag). The link between the variability of the AW current and the wind-driven surface circulation is further confirmed by the pattern emerging from the regression of the mean velocities within the AW layer upon PC2, which shows coherent variations of the boundary current all along the slope in the Canadian Basin. Note that the correlations tend to increase when we apply a 12 month running mean to the different time series (R between -0.5 and -0.6 compared to values between -0.4 and -0.5 without any running mean), while the opposite effect occurs for the correlations between the Fram Strait transport and the AW current (R decreases from values between 0.5 and 0.8 to values between 0.4 and 0.7). This suggests that short-term variability of the AW current in the Canadian Basin is likely driven by the variability of the inflow, while the longer timescales can be related to variations of the wind-driven surface circulation, consistent with the adjustment timescales discussed above.

The analysis of variability in the AW boundary current as simulated by the Drakkar hindcast suggests that the winds imprint their variability on the AW layer in the Canadian Basin, both remotely over the Nordic and Barents Sea (through forcing of the inflow to the Arctic Basin) and locally over the Canadian Basin (through forcing of the wind-driven Beaufort Gyre). However, the correlation analysis we performed does not allow a proper causal attribution of the link between the wind forcing and the AW current intensity. We thus complement this analysis with simulations performed with an idealized process model (Figure 1).

4. Results From the Circular Basin Process Model

Figure 4 shows time series of the maximum surface stress and AW inflow applied to the idealized process model, along with the resulting intensity of the circulation in the surface layer (approximated by the SSH at the center of the basin) and the intermediate layer (approximated by the northward flow of water warmer than 0°C on the eastern side of the basin, a quarter of the way around the basin perimeter). The temperature criteria ensure that we eliminate the small part of the AW current in the surface layer which is in direct contact with the atmosphere. In order to examine the variability of the different simulations, we discuss the departure of our three sensitivity runs from the *Control* run (blue lines in Figure 4).

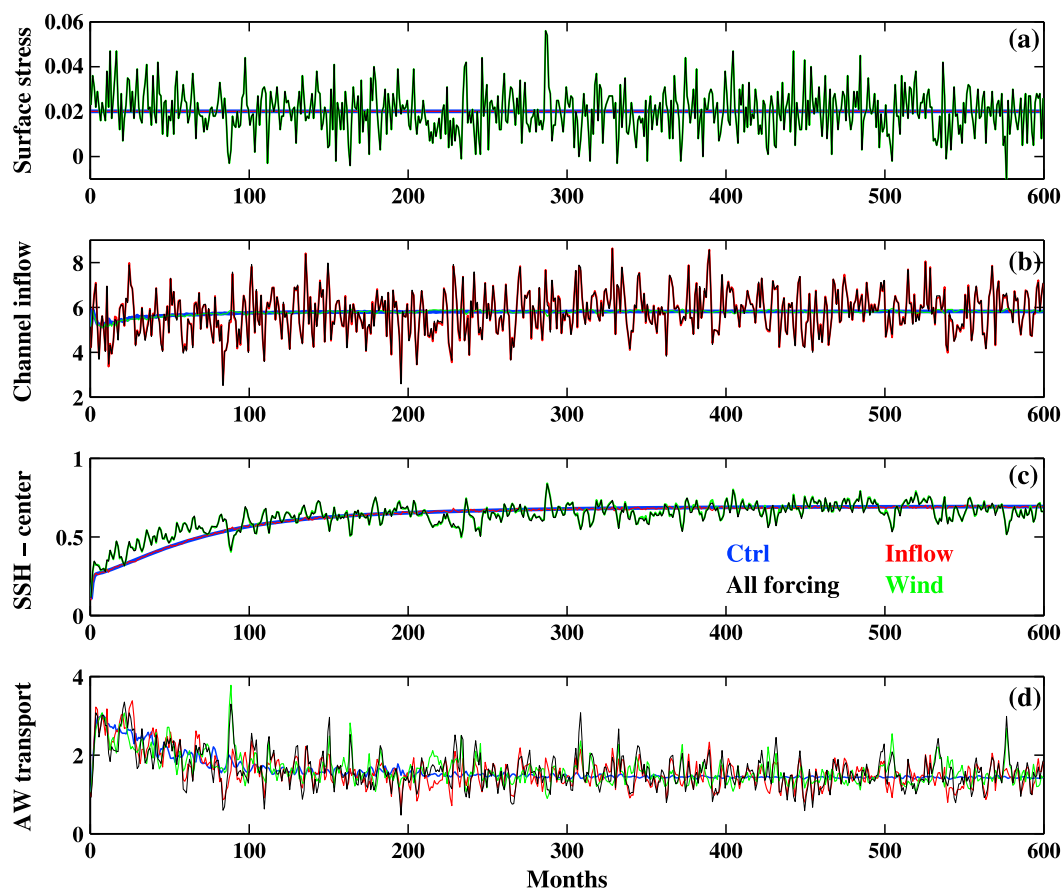


Figure 4. Time series for the four sensitivity experiments performed with the idealized model of (a) the surface stress (in N m^{-2}), (b) the inflow through the channel (in Sv), (c) the SSH at the center of the circular basin, and (d) the transport of the AW current (in Sv).

The SSH time series exhibit significant (and identical) variability for the two model runs forced with a variable surface stress (*Wind* and *All forcing*), while in the other two runs (*Control* and *Inflow*) there is no variability but simply a long decadal adjustment, similar to the adjustment discussed in *Davis et al.* [2014] and *Lique et al.* [2015]. The correlation between the surface stress and SSH anomalies (with respect to the *Control* run) is 0.63 for the *Wind* and *All forcing* runs (maximum without any lag). A spectral analysis of the time series (not shown) shows that the variations in SSH exhibit a reduced amount of energy at high frequencies (higher than 6 months) compared to the flat spectrum of the surface stress (which is forced with white noise). This reddening of the spectrum suggests that the dynamics of the Beaufort Gyre (i.e., its adjustment processes and the timescale on which they operate) are acting as a low-pass filter for the ocean surface stress variations.

The intensity of the AW current has a similar level of variability in each of the three sensitivity runs (standard deviations of 0.3–0.4 Sv). The *Control* run also shows some variability (standard deviation of 0.1 Sv after the initial adjustment), suggesting that part of the variability in the AW current arises from intrinsic variability, likely due to small-scale structure within the AW current core along the slope, due to the existence of eddies, meanders and shifts of the current core.

For the *All forcing* run, the AW current time series is significantly correlated with both the inflow through the channel ($R = 0.7$) and the SSH in the center of the basin ($R = -0.5$), with correlation coefficients that are somewhat similar to those in the *Drakkar* hindcast and again maximum without any lag. Interestingly, the time series of AW boundary current anomalies (relative to the *Control* run) in the *Wind* and *Inflow* experiments sum up almost linearly to the anomalies in the *All forcing* run, and thus the variability found in the *All forcing* run can be attributed to either variability in the surface stress or variability in the inflow. As a result, the variance of the AW transport in the *All forcing* experiment (0.17 Sv^2) results approximately from the sum of two terms of similar amplitudes, which are 0.1 Sv^2 and 0.08 Sv^2 for the *Inflow* and *Wind* runs, respectively. When variability

is only applied to the inflow to the basin, the variations of the AW current follow closely the variations of the inflow, with a correlation between the two time series of 0.9, maximum without any lag. Such a high correlation is expected as the boundary current adjusts quickly (within a month) to a change in its primary forcing (i.e., the channel inflow), through the propagation of boundary-trapped waves along the slope [Lique *et al.*, 2015]. In contrast, in the *Wind* run, variations in the AW current intensity match closely the variation of SSH in the center of the basin ($R = -0.8$), which again results from the surface stress variations albeit reddened and modified by the adjustment processes. As a result, the correlations between the AW current intensity and the SSH variations are -0.7 and -0.4 in the *Wind* and *All forcing* runs, respectively, while the same correlations computed with the stress variations rather than the SSH are only -0.4 and -0.3 . This reflects the imprint of the wind forcing variations over the basin, modulated by the surface circulation, onto the AW current.

5. Concluding Discussion

Despite the isolation of the Arctic Ocean's AW layer from the atmosphere by a fresh surface layer, observations have revealed that velocities within this intermediate layer exhibit large variability in time [e.g., Dmitrenko *et al.*, 2008; Ivanov *et al.*, 2009]. In the present study, we examine results from an ocean/sea ice model hind-cast, complemented by an idealized process model, in order to investigate the forcing mechanism of the AW circulation variability in the Canadian Basin, with a focus on the role of the wind. We build upon the previous study of Lique *et al.* [2015], for which the process model was initially developed to dissect the mechanisms explaining the interplay between the circulation in the surface and AW layers of the Arctic Ocean.

Results from the two numerical models suggest that variability in the AW boundary current is forced by the wind, through two distinct mechanisms which operate at different locations (i.e., within the Canadian Basin itself and remotely). First, part of the AW current variability is a direct and fast response to variability of the inflow into the Arctic Basin, which is itself forced by variability in the wind over the Nordic and Barents Seas. As the AW current adjusts quickly to a change of the inflow (i.e., on timescales less than a month), the velocity within the AW layer exhibits some coherent variations all along the slope around the Arctic Basin [Lique and Steele, 2012]. Second, the AW current in the Canadian Basin also carries some imprint of the variability in the ocean surface stress (which results from the wind and the sea ice conditions) over the Canadian Basin itself. Here the forcing occurs through a two-step process: the Beaufort Gyre in the surface layer acts as a low-pass filter for the surface stress variations (smoothing out frequencies higher than 6 months in our process model), and transmits its own variations to the AW current.

It is interesting, yet puzzling, that the circulation in the surface layer exhibits some high-frequency variations, while the adjustment process to a change of forcing described in Davis *et al.* [2014] and Lique *et al.* [2015] involves the balance between the Ekman pumping and an eddy-induced volume flux toward the boundary, and occurs over a decadal timescale. We would therefore expect the circulation to only respond to relatively long term changes in wind forcing (or ocean surface stress). Here we find that the Beaufort Gyre does act as a low-pass filter for the variations of the surface stress, yet the cutoff period (~ 6 months) is much shorter than expected. More work is required to fully explain this mismatch, but one possible explanation is that the model has a resolution too coarse to resolve the small Rossby radius of the Arctic Basin [Nurser and Bacon, 2014], and consequently only partially captures the mesoscale activity. Longer integrations (of order hundred years) would also be required to examine the variations of the circulation on decadal and longer timescales.

AW plays a key role for the thermal balance of the Arctic Ocean, and its variability on seasonal-to-multidecadal timescales has been the focus of numerous studies [e.g., Polyakov *et al.*, 2004; McLaughlin *et al.*, 2009; Lique and Steele, 2012]. However, many of these studies focus primarily on the temperature variations, while changes in the circulation pattern and intensity might play a bigger role for the Arctic heat budget variability [Lique and Steele, 2013; Itkin *et al.*, 2014]. Here we have linked the variability (or at least part of it) found in the AW boundary current with the local and remote wind forcing and confirmed the importance of the surface layer circulation to modulate the intensity of the circulation in the AW layer on longer timescales. It is still not clear, however, how the variability found in the boundary current is transmitted to the interior of the basin, and whether or not the heat content in the boundary and the interior of the Arctic Basin vary on the same timescale. Combining insight from process and state-of-the-art models should allow a better identification of the processes at play and the timescales on which they operate.

Acknowledgments

This study was funded by the UK Natural Environment Research Council (NERC) and is a contribution to the TEA-COSI project. The hindcast was carried out within the European DRAKKAR project, and the model outputs were kindly provided by J.M. Molines.

References

- Aagaard, K., L. Coachman, and E. Carmack (1981), On the halocline of the Arctic Ocean, *Deep Sea Res., Part I*, 28, 529–545, doi:10.1016/0198-0149(81)90115-1.
- Aksenov, Y., V. V. Ivanov, A. J. G. Nurser, S. Bacon, I. V. Polyakov, A. C. Coward, A. C. Naveira-Garabato, and A. Beszczynska-Moeller (2011), The Arctic circumpolar boundary current, *J. Geophys. Res.*, 116, C09017, doi:10.1029/2010JC006637.
- Barnier, B., et al. (2006), Impact of partial steps and momentum advection schemes in a global ocean circulation model at eddy permitting resolution, *Ocean Dyn.*, 56, 543–567, doi:10.1007/s10236-006-0082-1.
- Brodeau, L., B. Barnier, T. Penduff, A. M. Treguier, and S. Gulev (2010), An ERA40-based atmospheric forcing for global ocean circulation models, *Ocean Modell.*, 31, 88–104, doi:10.1016/j.ocemod.2009.10.005.
- Clement-Kinney, J. C., W. Maslowski, Y. Aksenov, B. de Cuevas, J. Jakacki, A. Nguyen, R. Osinski, M. Steele, R. A. Woodgate, and J. Zhang (2014), On the flow through Bering Strait: A synthesis of model results and observations, in *The Pacific Arctic Region*, pp. 167–198, Springer, Netherlands.
- Coachman, L. K., and C. A. Barnes (1963), The movement of Atlantic water in the Arctic Ocean, *J. Arct. Inst. North Am.*, 16, 8–16.
- Davis, P. E. D., C. Lique, and H. L. Johnson (2014), On the link between Arctic sea ice decline and the freshwater content of the Beaufort Gyre: Insights from a simple process model, *J. Clim.*, 27, 8170–8184, doi:10.1175/JCLI-D-14-00090.1.
- Dmitrenko, I. A., I. V. Polyakov, S. A. Kirillov, L. A. Timokhov, I. E. Frolov, V. T. Sokolov, H. L. Simmons, V. V. Ivanov, and D. Walsh (2008), Toward a warmer Arctic Ocean: Spreading of the early 21st century Atlantic Water warm anomaly along the Eurasian Basin margins, *J. Geophys. Res.*, 113, C05023, doi:10.1029/2007JC004158.
- Dmitrenko, I. A., B. Rudels, S. A. Kirillov, Y. O. Aksenov, V. S. Lien, V. V. Ivanov, U. Schauer, I. V. Polyakov, A. Coward, and D. J. Barber (2015), Atlantic water flow into the Arctic ocean through the St. Anna Trough in the northern Kara Sea, *J. Geophys. Res. Oceans*, 120, 5158–5178, doi:10.1002/2015JC010804.
- Fieg, K., R. Gerdes, E. Fahrbach, A. Beszczynska-Möller, and U. Schauer (2010), Simulation of oceanic volume transports through Fram Strait 1995–2005, *Ocean Dyn.*, 60, 491–502, doi:10.1007/s10236-010-0263-9.
- Guthrie, J. D., J. H. Morison, and I. Fer (2013), Revisiting internal waves and mixing in the Arctic Ocean, *J. Geophys. Res. Oceans*, 118, 3966–3977, doi:10.1002/jgrc.20294.
- Itkin, P., M. Karcher, and R. Gerdes (2014), Is weaker Arctic sea ice changing the Atlantic water circulation?, *J. Geophys. Res. Oceans*, 119, 5992–6009, doi:10.1002/2013JC009633.
- Ivanov, V., I. Polyakov, I. Dmitrenko, E. Hansen, I. Repina, S. Kirillov, C. Mauritzen, H. Simmons, and L. Timokhov (2009), Seasonal variability in Atlantic Water off Spitsbergen, *Deep Sea Res., Part I*, 56, 1–14.
- Karcher, M., F. Kauker, R. Gerdes, E. Hunke, and J. Zhang (2007), On the dynamics of Atlantic Water circulation in the Arctic Ocean, *J. Geophys. Res.*, 112, C04S02, doi:10.1029/2006JC003630.
- Karcher, M., J. N. Smith, F. Kauker, R. Gerdes, and W. M. Smethie Jr. (2012), Recent changes in Arctic Ocean circulation revealed by iodine-129 observations and modeling, *J. Geophys. Res.*, 117, C08007, doi:10.1029/2011JC007513.
- Koldunov, N. V., et al. (2014), Multimodel simulations of Arctic Ocean sea surface height variability in the period 1970–2009, *J. Geophys. Res. Oceans*, 119, 8936–8954, doi:10.1002/2014JC010170.
- Lique, C., and M. Steele (2012), Where can we find a seasonal cycle of the Atlantic water temperature within the Arctic Basin?, *J. Geophys. Res.*, 117, C03026, doi:10.1029/2011JC007612.
- Lique, C., and M. Steele (2013), Seasonal to decadal variability of Arctic Ocean heat content: A model-based analysis and implications for autonomous observing systems, *J. Geophys. Res. Oceans*, 118, 1673–1695, doi:10.1002/jgrc.20127.
- Lique, C., A. M. Treguier, M. Scheinert, and T. Penduff (2009), A model-based study of ice and freshwater transport variability along both sides of Greenland, *Clim. Dyn.*, 33, 685–705, doi:10.1007/s0038200805107.
- Lique, C., A. M. Treguier, B. Blanke, and N. Grima (2010), On the origins of water masses exported along both sides of Greenland: A Lagrangian model analysis, *J. Geophys. Res.*, 115, C05019, doi:10.1029/2009JC005316.
- Lique, C., J. D. Guthrie, M. Steele, A. Proshutinsky, J. H. Morison, and R. Krishfield (2014), Diffusive vertical heat flux in the Canada Basin of the Arctic Ocean inferred from moored instruments, *J. Geophys. Res. Oceans*, 119, 496–508, doi:10.1002/2013JC009346.
- Lique, C., H. L. Johnson, and P. E. D. Davis (2015), On the interplay between the circulation in the surface and the intermediate layers of the Arctic Ocean, *J. Phys. Oceanogr.*, 45, 1393–1409, doi:10.1175/JPO-D-14-0183.1.
- Madec, G. (2008), NEMO Ocean engine, Note du pôle modélisation 27, Institut Pierre-Simon Laplace (IPSL), Paris, France.
- Marshall, J., A. Adcroft, C. Hill, L. Perelman, and C. Heisey (1997), A finite-volume, incompressible Navier Stokes model for studies of the ocean on parallel computers, *J. Geophys. Res.*, 102, 5753–5766, doi:10.1029/96JC02775.
- McLaughlin, F. A., E. C. Carmack, W. J. Williams, S. Zimmermann, K. Shimada, and M. Itoh (2009), Joint effects of boundary currents and thermohaline intrusions on the warming of Atlantic water in the Canada Basin, 1993–2007, *J. Geophys. Res.*, 114, C00A12, doi:10.1029/2008JC005001.
- Nurser, A. J. G., and S. Bacon (2014), The Rossby radius in the Arctic Ocean, *Ocean Sci.*, 10, 967–975, doi:10.5194/os-10-967-2014.
- Peralta-Ferriz, C., J. H. Morison, J. M. Wallace, and J. Zhang (2011), A basin-coherent mode of sub-monthly variability in Arctic Ocean bottom pressure, *J. Geophys. Res. Lett.*, 38, L14606, doi:10.1029/2011GL048142.
- Peralta-Ferriz, C., J. H. Morison, J. M. Wallace, J. A. Bonin, and J. Zhang (2014), Arctic Ocean circulation patterns revealed by GRACE, *J. Clim.*, 27, 1445–1468, doi:10.1175/JCLI-D-13-00013.1.
- Polyakov, I. V., G. V. Alekseev, L. A. Timokhov, U. S. Bhatt, R. L. Colony, H. L. Simmons, D. Walsh, J. E. Walsh, and V. F. Zakharov (2004), Variability of the intermediate Atlantic water of the Arctic Ocean over the last 100 years, *J. Clim.*, 17, 4485–4497, doi:10.1175/JCLI-3224.1.
- Popova, E. E., A. Yool, A. C. Coward, Y. K. Aksenov, S. G. Alderson, B. A. de Cuevas, and T. R. Anderson (2010), Control of primary production in the Arctic by nutrients and light: Insights from a high resolution ocean general circulation model, *Biogeosciences*, 7, 3569–3591, doi:10.5194/bg-7-3569-2010.
- Rippeth, T. P., B. J. Lincoln, Y.-D. Lenn, J. A. M. Green, A. Sundfjord, and S. Bacon (2015), Tide-mediated warming of Arctic halocline by Atlantic heat fluxes over rough topography, *Nat. Geosci.*, 8, 191–194, doi:10.1038/ngeo2350.
- Rudels, B., L. G. Anderson, and E. P. Jones (1996), Formation and evolution of the surface mixed layer and halocline of the Arctic Ocean, *J. Geophys. Res.*, 101, 8807–8822, doi:10.1029/96JC00143.
- Rudels, B., H. J. Friedrich, and D. Quadfasel (1999), The Arctic circumpolar boundary current, *Deep Sea Res., Part II*, 46, 1023–1062, doi:10.1016/S0967-0645(99)00015-6.
- Rudels, B., M. Korhonen, U. Schauer, S. Pisarev, B. Rabe, and A. Wisotzki (2015), Circulation and transformation of Atlantic water in the Eurasian Basin and the contribution of the Fram Strait inflow branch to the Arctic Ocean heat budget, *Prog. Oceanogr.*, 132, 128–152, doi:10.1016/j.pocean.2014.04.003.

- Schauer, U., A. Beszczynska-Möller, W. Walczowski, E. Fahrbach, J. Piechura, and E. Hansen (2008), Variation of measured heat flow through the Fram Strait between 1997 and 2006, in *Arctic–Subarctic Ocean Fluxes*, edited by R. R. Dickson, J. Meincke, and P. Rhines, pp. 385–404, Springer, Netherlands.
- Shaw, W. J., and T. P. Stanton (2014), Vertical diffusivity of the Western Arctic Ocean halocline, *J. Geophys. Res. Oceans*, *119*, 5017–5038, doi:10.1002/2013JC009598.
- Spall, M. A. (2013), On the circulation of Atlantic water in the Arctic Ocean, *J. Phys. Oceanogr.*, *43*, 2352–2371, doi:10.1175/JPO-D-13-079.1.
- Steele, M., R. Morley, and W. Ermold (2001), PHC: A global ocean hydrography with a high quality Arctic Ocean, *J. Clim.*, *14*, 2079–2087, doi:10.1175/1520-0442(2001)014<2079:PAGOHW>2.0.CO;2.
- Tsubouchi, T., S. Bacon, A. C. Naveira Garabato, Y. Aksenov, S. W. Laxon, E. Fahrbach, A. Beszczynska-Möller, E. Hansen, C. M. Lee, and R. B. Ingvaldsen (2012), The Arctic Ocean in summer: A quasi-synoptic inverse estimate of boundary fluxes and water mass transformation, *J. Geophys. Res.*, *117*, C01024, doi:10.1029/2011JC007174.
- Turner, J. S. (2010), The melting of ice in the Arctic Ocean: The influence of double-diffusive transport of heat from below, *J. Phys. Oceanogr.*, *40*, 249–256, doi:10.1175/2009JPO4279.1.
- Yang, J. (2005), The Arctic and subarctic ocean flux of potential vorticity and the Arctic Ocean circulation*, *J. Phys. Oceanogr.*, *35*, 2387–2407, doi:10.1175/JPO2819.1.